Full Length Research Article
Advancements in Life Sciences – International Quarterly Journal of Biological Sciences

ARTICLE INFO

Date Received: 09/01/2024;
Date Revised: 25/03/2024;
Available Online: 18/04/2024;

Open Access

Iron-Based Nanoparticles Synthesis, Characterization, and Antimicrobial Effectiveness

Hisham Faiz Jaha[1]*, Yasir Anwar[1,2], Saleh M. Al-Maaqar[1,3], Tahseen Kamal[4], Sher Bahadar Khan[5]

Author's Affiliation:
1. Department of Biological Sciences, Faculty of Science, King Abdulaziz University Jeddah - Saudi Arabia
2. Center of Excellence in Bionanoscience Research, King Abdul Aziz University, Jeddah - Saudi Arabia
3. Faculty of Education, Department of Biology, Albaydha University, Al-Baydha - Yemen
4. Center of Excellence for Advanced Materials Research, King Abdulaziz University, P. O. Box 80203 Jeddah 21589 - Saudi Arabia
5. Chemistry Department, Faculty of Science, King Abdulaziz University, P.O. Box 80203, Jeddah 21589 - Saudi Arabia

***Corresponding Author:**
Hisham Faiz Jaha
Email: malalosy@uowasit.edu.iq

How to Cite:
Jaha HF, Anwar Y, Al-Maaqar SM, Kamal T, Khan SB (2024). Iron-Based Nanoparticles Synthesis, Characterization, and Antimicrobial Effectiveness. Adv. Life Sci. 11(2): 525-532.

Keywords:
Antibacterial; Antifungal Agents; Iron; Silver; Chitosan; Nanoparticles

Abstract

Background: Antimicrobial resistance (AMR) has emerged as a significant and pressing public health concern, posing serious challenges to effectively preventing and treating persistent diseases. Developing new antibiotics with different mechanisms of action is crucial to effectively address challenges in treating infections. A lot of work has already been done on mono-metallic nanoparticles to address the issue.

Methods: This study aimed to synthesize multi-metallic iron, silver, and chitosan-embedded nanoparticles using a green approach. Iron, silver, chitosan nanoparticles, and a composite of iron–silver–chitosan was also synthesized. The synthesized nanoparticles and composites were characterized through X-ray diffraction (XRD), scanning electron microscopy (SEM), energy-dispersive X-ray spectroscopy (EDX), and Fourier Transform Infrared Spectroscopy (FTIR) to evaluate their structural parameters. Their antimicrobial efficacy was investigated through MIC (minimum inhibitory concentration), MBC (minimum bactericidal concentration), and well-disk diffusion assays against *Pseudomonas aeruginosa, Acinetobacter baumannii*, *Staphylococcus aureus*, *Staphylococcus epidermidis* and *Candida albicans.*

Results: The size of the Cu-NPs, Cu-Ag NPs, and Cu-Ag-CS NPs were found to be in the range of 32-40 nm size with a spherical shape. The nanocomposites' MIC and MBC were calculated to be 125 µg/mL and 500 µg/mL, respectively. The nanocomposites exhibited a range of clear inhibition zones, with a minimum diameter of 12 ± 0.5 mm and a maximum diameter of 22 ± 0.5 mm.

Conclusion: The iron–silver–chitosan nanocomposite has been shown to have significant antimicrobial effects in the laboratory environment compared to other nanoparticles hence can be applied as potential biomedical/biological candidates in future.

Introduction

Antimicrobial Resistance (AMR) is a global threat where microorganisms adapt and grow in the presence of medications, rendering them ineffective. This poses serious challenges to public health systems worldwide. Infections with AMR lead to severe illnesses, longer hospital stays, increased healthcare costs, and treatment failures [1]. Europe spends over nine billion euros annually on AMR-related expenses, and the United States incurs an additional 20 billion dollars in healthcare costs and a productivity loss of around 35 billion dollars per year [2-4]. Bacterial and fungal infections have posed significant challenges to human health for centuries and are the leading cause of human mortality. The future of healthcare is uncertain as infectious diseases become untreatable with antibiotics. Antibiotics have played a crucial role in controlling infectious diseases and reducing mortality rates [5]. However, the use of antibiotics, whether bactericidal or bacteriostatic, has exerted selective pressure on bacteria, leading to the development of drug resistance in certain pathogens [6-8]. Unfortunately, the development of new antibiotics is slow, and the existing ones have limitations, contributing to the rise of drug resistance and the emergence of new multidrug-resistant species [9]. In many cases, the resistant bacteria become resistant to multiple drugs, making patients more vulnerable to infections and resulting in prolonged suffering. Therefore, the development of novel antibiotics with various mechanisms of action is essential to address these challenges.

Currently, there is a growing focus on developing effective chemical treatments and probiotic therapies for microbial diseases. In addition to these approaches, extensive research has been conducted on the use of metal nanoparticles in disease treatment, yielding promising outcomes [10,11]. Various types of nanoparticles, including silver, copper, iron, graphene, zinc oxide, and polymer nanoparticles such as chitosan, have been studied in this regard [12-14]. Moreover, alloy and silver nanoparticles, iodine, and copper-based materials have also been investigated for their potential effects on various microorganisms [15-17].

The antimicrobial properties of iron have been studied. Ismail's study in 2015 revealed that magnetic iron oxide nanoparticles effectively hindered the growth of both Gram-positive bacteria (specifically *Staphylococcus aureus*) and Gram-negative bacteria (including *Escherichia coli, Pseudomonas aeruginosa*, and *Serratia marcescens*) [18]. Similarly, Pal in 2014 demonstrated the toxic effects of iron oxide nanoparticles on *Bacillus subtilis* and *Escherichia coli* [19]. Pal's research indicated that modifying the nanoparticle surface with chitosan reduced its toxicity [19]. In a separate study conducted by Mohan in 2019, a comparison was made between iron oxide nanoparticles synthesized through biological and chemical methods [20]. Silver nanoparticles, often referred to as silver, predominantly consist of silver oxide because of a high proportion of silver atoms on the surface compared to bulk. Subject to the desired application, various forms of nanoparticles can be produced, with spherical silver nanoparticles being commonly employed. These silver nanoparticles have demonstrated significant antibacterial characteristics against both Gram-positive and Gram-negative bacteria [21,22], and fungi such as *Candida albicans* [23]. Chitosan nanocomposites have shown promise as antimicrobial agents. Chitosan, a biopolymer derived from chitin, possesses inherent antimicrobial properties due to its cationic nature. When incorporated into nanocomposites, chitosan can enhance its antimicrobial activity and expand its applications [12,24]. Chitosan nanocomposites can be prepared by incorporating various antimicrobial agents, such as metal nanoparticles (e.g., silver, copper), metal oxides (e.g., zinc oxide), or other organic antimicrobial agents [12,25,26]. These agents can be dispersed within the chitosan matrix or deposited onto its surface, resulting in enhanced antimicrobial properties. The antimicrobial activity of chitosan nanocomposites is attributed to multiple mechanisms. The cationic amino groups of chitosan interact with the anionic microbial cell membranes, resulting in the membrane disruption and leakage of intracellular components [14]. Hence, the development of novel antibiotics with alternative mechanisms of action holds the potential to address these challenges effectively. In the broader context, iron, silver, and chitosan nanoparticles have demonstrated significant biological activities, offering promising applications in medicine and biotechnology. Exploring the biological properties of these nanoparticles is crucial for advancing the development of innovative therapeutic approaches for the treatment of bacterial and fungal infections, cancer, and other diseases.

Most of the study is being carried out using monometallic nanoparticles and their use in biological efficacy. Hence, considering the importance of the subject, this study aimed to synthesize some green multi-metallic novel nanoparticles that can offer cost-effectiveness and high-performance biological efficacies. We synthesized chitosan-embedded iron and copper nanoparticles, and their structural parameters were evaluated using various techniques such as SEM, XRD, EDX, and FTIR. Furthermore, the biological applications of the characterized nanocomposites, including their antibacterial, and antifungal activities,

were investigated to evaluate the efficacy for biological applications.

Methods

Synthesis of Iron NPs

Iron nanoparticles were prepared by the chemical precipitation of Fe (II) and Fe (III) ions through urea for which 0.02M solution of $FeCl_2.4H_2O$ (99%) and 0.05% $FeCl_3.6H_2O$ (99%) solution were made in distilled water to main the 1:2 molar ratios between the two ions. 20mL of both solutions were mixed in a container and 99% urea (NH_2CONH_2) solution as a precipitating agent was added into the reaction mixture in a 1:2 molar ratio with the mixture. The mixture solution was kept under constant stirring for 12 hours at room temperature. The precipitates were filtered out, washed in ethanol, and dried [27].

Synthesis of Silver NPs

The silver nanoparticles were synthesized through the chemical reduction of AgNO3 using NaBH4 as a reducing agent. 40mL of AgNO3 solution was made in the distilled water and kept under vigorous stirring. Then, 1.5mL of ice-cooled NaBH4 solution (0.8 mol/L) was added dropwise to the AgNO3 solution, and stirring was continued. After adding $NaBH_4$, the solution turned bright yellow immediately upon the formation of silver NPs. Precipitates were separated, washed, and dried in open air [28].

Synthesis of Nanocomposites

Two composites of iron NPs were made, one incorporating silver NPs and the other with the inclusion of silver and chitosan. To prepare iron-silver nanocomposite, the above-prepared salt solutions were mixed in 9:1 for iron and silver respectively. The mixture solution was heated at 95°C under constant stirring until the precipitates were formed which were separated, washed, and dried. To prepare the chitosan NPs, 2.5 g of pure chitosan was dissolved in the 250 mL of 1% acetic acid and 10mL of aq. solution of NaNO2 was added to it to depolymerize the polymeric structure of chitosan. The mixture solution was kept under vigorous stirring for 1 hour and a solution of sodium hydroxide was added to precipitate the chitosan NPs which were centrifuged and washed with the distilled water various times. The obtained chitosan NPs were freeze-dried and kept in a dry place.

To investigate the effect of chitosan and silver addition on the morphology, size, and phase composition of iron NPs, a composite of iron, silver, and chitosan was synthesized. To prepare the nanocomposite, the above-prepared solution of iron chloride and silver chloride was mixed with the chitosan acetic solution in a certain ratio for 10 h under constant mixing. The mixture solution was subjected to heat at 80-95°C and continuously stirred until the resultant NPs were precipitated out. The precipitates were filtered out, washed, and dried for further use [29].

Pathogenic Bacteria and Fungal Strains

Pseudomonas aeruginosa (P. aeruginosa), *Acinetobacter baumannii (A. baumannii, Staphylococcus aureus (S. Aureus)* , *Staphylococcus epidermidis (S. epidermidis), Candida albicans*(*C. albicans*) were obtained from Microbiology Laboratory, Department of Biology, King Abdulaziz University, Jeddah, KSA.

Susceptibility of Pathogenic Bacteria to Nanoparticles Minimum Inhibition Concentration (MIC)

To determine their lowest inhibitory concentration, samples of nanoparticles (Fe-NPs, Fe–Ag NPs, and Fe–Ag-CS NPs) that demonstrated antimicrobial activity during antibacterial screening underwent additional testing. Mostly, 96-well microtiter plates are utilized in micro-broth dilution tests to estimate the MICs. To calculate the MICs of NPs against the examined bacteria, the MICs were done using the micro-diluted broth approach as outlined by NCCLS (Wikler 2006). At 37°C, the incubation was carried out for 24 hours. 5 µl of Resazurin sodium salt dye solution (R7017 Sigma-Aldrich) was added to each well after incubation. Column 11, which only contains media, attests that there was no plate contamination through dish preparation. Column 12 represents a positive control that only has cultivated strains. In contrast, columns 1 through 10 represent the serial dilution of NPs with media from 1mg/ml to 0.0019 mg/ml. This method assists in producing precise MIC values while overcoming significant issues with color and solubility that could obstruct growth evaluations for several substances [30].

Estimation of Minimal Bactericidal Concentration (MBC)

The minimal bactericidal concentrations (MBC) are the lowest concentration of the samples treated with Fe-NPs, Fe–Ag NPs, and Fe–Ag-CS NPs at which inoculated bacteria were killed. Then, spreading 10 µl of medium from the MIC's microplate contents, which showed no bacterial growth, and it was re-inoculated on nutrient agar plates followed by incubation at 37°C for 24 hours. The first well with colony counts of <5 was considered negative for growth and reported as the MBC [31]

Disk Diffusion Method

Mueller Hinton Agar Media (MHA) was utilized as the growth medium, and it was inoculated with bacterial strains at the concentration of 10^6 colony-forming

units per milliliter (CFU/mL). Subsequently, 7-mm paper filter discs were impregnated with Fe-NPs, Fe–Ag NPs, and Fe–Ag-CS NPs at a concentration of 1mg/ml, which was then placed on the agar. As a negative control, sterile distilled water (SDW) was used. The nanoparticles were subjected to diffuse into the medium at room temperature for 30 minutes. Plates were then incubated for 24h at 37 °C. The average and standard deviation (SD) of three independent trials were calculated to determine the zone of inhibition.

Results

Characterization of NPs

Powder X-Ray Diffraction (PXRD) Analysis

Powder XRD patterns of iron and its nanocomposites (iron-silver and iron-silver-chitosan) were analyzed to find out the phase composition, crystallite sizes, and defect levels in the powders. For recording the powder patterns, materials were grounded to the powder form, and data obtained was enlisted in Table 1. The powder XRD intensities at corresponding 2θ angles were given in PXRD patterns of the synthesized materials shown in Fig. 1.

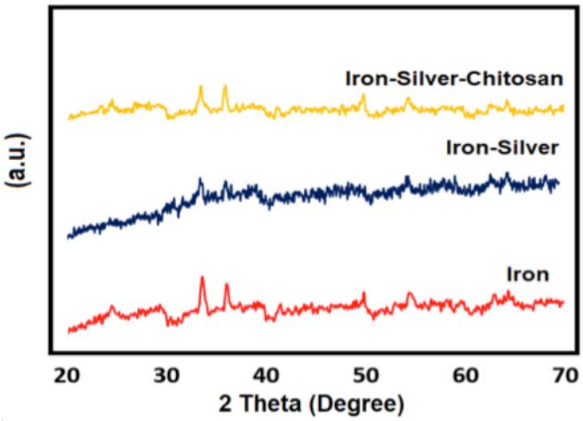

Figure 1: Powder XRD Pattern of Iron, Iron-Silver and Iron-Silver-Chitosan NPs Indicating Potential Crystal Planes.

The parameters like nanoparticle size, volume, dislocation densities, and microstrain were analyzed for iron and its nanocomposites from PXRD (Table 1). The crystallite size was calculated using the Debye Sherrer formula [32] given in Eq. 1 as follows:

$$\text{Crystallite Size (D)} = 0.91\lambda/\beta\cos\theta \qquad (1)$$

Where D is nanoparticle size, λ is the wavelength of 1.54Å Cu-Kα X-ray beam, the cos θ is the angle of diffraction and β is the value at full-width at half-maximum. The dislocation density (δ) was calculated by following Eq. 2. As follows:

$$\text{Dislocation Density } (\delta) = \frac{1}{D^2} \qquad (2)$$

Eq. 2 talks about the dislocation densities which determine the extent of defects in the synthesized NPs [33]. The volume (V) of synthesized nanocomposites and iron was calculated by following Eq. 3.

$$\text{Volume (V)} = D^3 \qquad (3)$$

Microstrain levels in the materials are calculated by following Eq. 4 as follows:

$$\text{Microstrain } (\varepsilon) = \frac{\beta}{4tan\theta} \qquad (4)$$

Samples	Average Crystallite Size (nm)	Volume $V=D^3$	Dislocation Density $(nm)^{-2}$ (δ)	Micro Strain (ε)	EDX Composition (%)
Iron	32.67±4	34869	1.53×10^4	0.027	Fe (99.62)
Iron-Silver	40.84±3	68117	1.22×10^4	0.014	Fe (99.08), Ag (0.20)
Iron-Silver-Chitosan	35.86±5	46113	1.39×10^4	0.017	Fe (98.94), Ag (0.31)

Table 1: Powder XRD Parameters i.e. Crystallite Size, Volume, Dislocation Density, Microstrain, and EDX Composition of Synthesized NPs.

Elemental Analysis by EDX

Elemental composition was analyzed by EDX for iron and its nanocomposites. The obtained percentages of the individual elements are reported in Table 1 and EDX images are depicted in Fig. S1 of supplemental data.

Scanning Electron Microscopic (SEM) Analysis

The surface morphological characters of the nanocomposites of iron were evaluated using SEM analysis and spectrographs obtained are shown in Fig. 2.

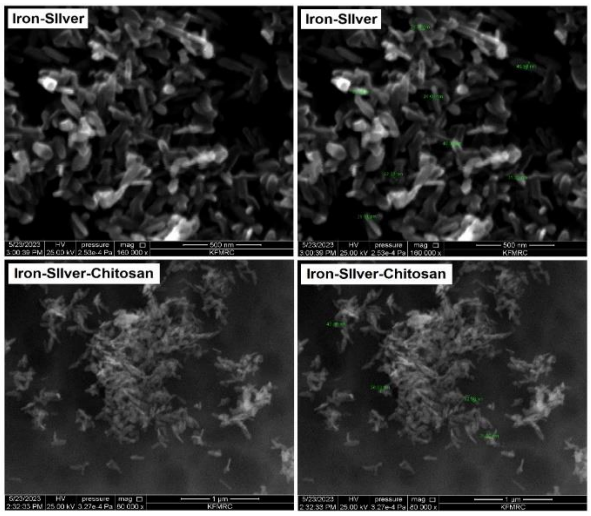

Figure 2: SEM Images of Iron-Silver, and Iron-Silver-Chitosan NPs Indicating Surface Morphology and Size.

FTIR Analysis

To evaluate the molecular interactions among chitosan, iron, and silver, FTIR analysis was carried out and the spectra obtained are depicted in Fig. S2 of

supplemental data. All the FTIR frequencies obtained are enlisted in Table 2.

Samples	Wavenumber (cm^{-1})	Vibration
Iron	3436.54	O-H stretching
	1550.59	N-H bending
	1359.67	C-O-C stretching
	913.61	Fe-O stretching
	527.18, 444.03	Fe-O stretching
Iron+Silver	3436.52	O-H stretching
	1556.02	N-H-bending
	1383.93	C-O-C stretching
	913.16	Fe-O stretching
	526.85, 443.59	Fe-O stretching
Iron+Silver+Chitosan	3497.69	O-H stretching
	1546.47	N-H-bending
	1364.24	C-O-C stretching
	917.31	C-H bending
	527.55, 445.27	Fe-O stretching

Table 2: The Wavenumber and Corresponding FTIR Vibrations of Iron, Iron-Silver, and Iron-Silver-Chitosan NPs.

Antibacterial Activity

In this study, the researchers aimed to explore the antibacterial effects of three types of nanoparticles: Iron-Silver-Chitosan NPs. These nanoparticles have shown potential in exerting antibacterial activity against a range of pathogens. The specific pathogens targeted in this study included *P. aeruginosa, A. baumannii, S. aureus, S. epidermidis,* and *C. albicans* . Both qualitative and quantitative methods were employed to assess the antibacterial efficacy of the nanoparticles. The researchers also analyzed quantitatively by determining the MIC and MBC in (Fig. S3 of supplemental data). The MIC is the lowest concentration of a substance (in this case, the nanoparticles) that can effectively inhibit bacterial growth. The bacterial growth was assessed by visually inspecting the turbidity of the broth after the addition of Resazurin dye. Results of MIC and MBC activities are presented in Fig 3 and 4.

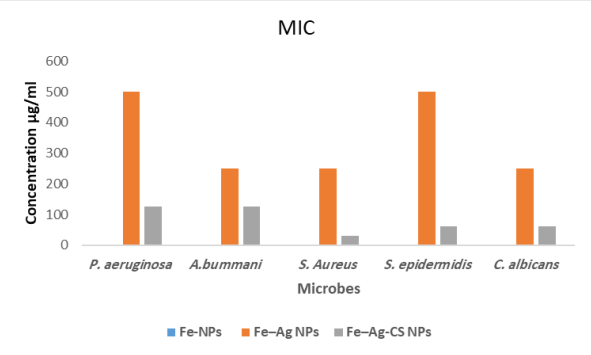

Figure 3: Determination of MIC for Bacterial Pathogens Treated with Fe-NPs, Fe-Ag NPs, and Fe-Ag-CS NPs.

Antibacterial Test Using Agar Disk Diffusion Assay

The disk-diffusion assay was used to evaluate the antimicrobial activity of different nanoparticles, namely Fe–Ag-CS NPs, against a range of pathogenic microbes including *Pseudomonas aeruginosa, Acinetobacter baumannii, Staphylococcus aureus, Staphylococcus epidermidis,* and *Candida albicans* (Fig. S4 of supplemental data). The results are presented in Fig. 5.

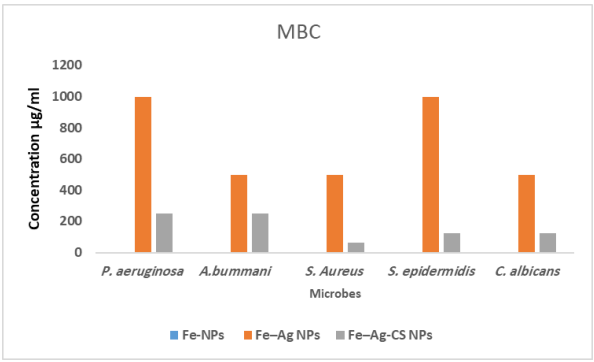

Figure 4: Determination of MBC for Bacterial Pathogens Treated with Fe-NPs, Fe–Ag NPs, and Fe–Ag-CS NPs.

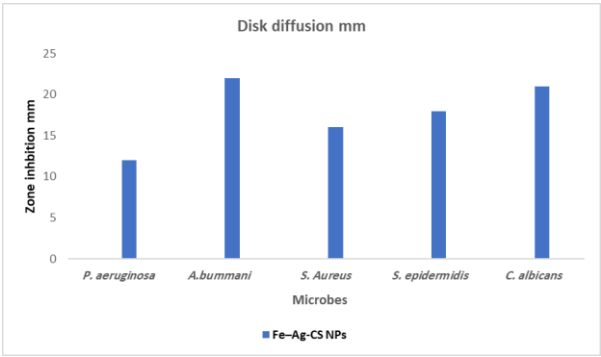

Figure 5: Inhibition Zone (mm) of Cu-NPs, Cu–Ag NPs, and Cu–Ag-CS NPs by Agar Disk Diffusion Method Against Bacterial Tested.

Discussion

In, powder XRD patterns, the iron has shown diffraction peaks at 33.70, 36.20, 49.85, and 54.68 2θ values in its PXRD pattern. The iron-silver composite has shown PXRD peaks at 33.79, 36.33, 54.40, 63.23, and 64.61 2θ values. While iron-silver-chitosan showed peak intensities at 33.49, 35.97, 49.85, 54.42, and 64.35 2θ values. The comparison of obtained powder XRD patterns of materials was made with the literature-reported standard powder patterns of Fe, Ag, and chitosan-based nanocomposites. Iron was found to be present as a major phase as most of the peak intensities corresponded to Fe NPs which can also be found through elemental composition of materials through EDX. For iron-silver and iron-silver-chitosan nanocomposites, slight peak shifts were observed which possibly ascribed to silver incorporation in the iron lattice planes and organic embeddedness of chitosan structure. The diffraction spectra of iron and its nanocomposites with silver and chitosan were compared with the standard powder patterns (JCPDS card, file No. 77-1545) [34] which shows an inverse

cubic spinel structure having (220), (400), (311), (422), (440), (511), and (533) lattice planes corresponds to iron based oxides crystal appeared in both bare and chitosan-based nanocomposites [35].

The PXRD parameters were calculated which enlisted in Table 1. The average crystallite size calculated for synthesized NPs at corresponding intensities was 32.67, 40.84, and 35.86 for iron, iron-silver, and iron-silver-chitosan respectively. The volume of the materials was found to be decreased when silver was incorporated and further decreased upon the addition of chitosan. The microstrain values in iron and its nanocomposites are ascribed to the strain-induced broadening in the crystals due to defectiveness and distortion in structural characteristics [36]. The values of microstrain and dislocation densities were found to be very low which shows very low defect value, higher stability, and very insignificant distortion/imperfections in synthesized NPs.

EDX results depicted the percentages of individual elements. In Fe nanoparticles, 99.62% iron was calculated indicating its presence as a major phase (as depicted by PXRD results) whereas, in the iron-silver nanocomposite, 99.08% of iron and 0.20% of silver were present. In the iron-silver-chitosan nanocomposite, 98.91% of iron and 0.31% of silver were present confirming the little incorporation of silver into the lattice structure of iron NPs. The EDX results were following the PXRD findings.

The SEM images of the iron-silver nanocomposite have shown not-so-elongated octahedral shapes with a relatively small number of nanoparticles having cuboidal morphology. The cubo-octahedral shape is more commonly known with iron oxide compounds reported by literature reports [27]. The iron+silver+chitosan nanocomposite has shown a short rod-like straw shape with little agglomeration among them which can be due to the chitosan interlinked structure. The iron and silver metal ions are supposed to be attached and embedded inside the chitosan polymer chains causing the change in morphology of the nanocomposite [37]. The width of iron-silver and iron-silver-chitosan varies from 28-49.5nm and 25.50-45.37nm respectively.

The FTIR spectra of iron and its nanocomposites have shown a characteristic broad band between 3436-3497 cm^{-1} that is ascribed to the axial deformation of -OH and the -NH stretching vibrations to overlap [28]. This peak intensity for all of the synthesized nanocomposites is ascribed to the overlap of O-H and N-H stretching vibration due to chitosan structural interaction [38]. All synthesized NPs have shown peaks in the range 525-527 cm^{-1} and 442-445 cm^{-1} which corresponds to the Fe-O stretching in all of the NPs. The chitosan structure also shows an N-H-bending in the range of 1546-1550 cm^{-1} and C-O-C stretching modes in the region of 1359-1383 cm^{-1} confirming the incorporation of chitosan polymeric matrix in synthesized nanocomposites [13]. The bands were not visible for silver incorporation in the FTIR spectra due to the low dopant concentration of silver in the crystal lattice planes of iron.

The minimum inhibitory concentration (MIC) values of Iron-Silver-Chitosan NPs against the studied pathogenic microbes ranged from 31 to 500 µg/mL (Fig. S3 of supplemental data). Antimicrobial activity of iron nanoparticles was not observed against pathogenic microorganisms. On the other hand, Fe–Ag nanoparticles exhibited the lowest MIC of 250 µg/mL against *S. aureus, C. albicans*, and *A. baumannii*, while the highest MIC observed was 500 µg/mL against *S. epidermidis* and *P. aeruginosa* (Fig. 3). The MBC of Fe–Ag nanoparticles was twice the MIC value, indicating their greater potency in killing the microorganisms (Fig. 3). In the case of Fe-Ag-Ch nanoparticles, the lowest MIC recorded was 31 µg/mL against *S. aureus*, followed by *S. epidermidis* and *C. albicans* at 62 µg/mL, while the highest MIC observed was 125 µg/mL against *P. aeruginosa and A. baumannii* (Fig. 6). Fe–Ag-CS nanoparticles, the MBC was higher than the MIC, suggesting that the nanoparticles can effectively eliminate bacteria at higher concentrations (Fig. 4).

For antibacterial test using agar disk diffusion assay, the results revealed varying inhibition zones, indicating the extent of antimicrobial efficacy exhibited by the nanoparticles. The inhibition zones ranged from a minimum of 12 ±0.5 mm to a maximum of 22 ±0.5 mm, providing valuable insights into the potency of the nanoparticles against the tested pathogens. The maximum antimicrobial activity was observed against *A. baumannii* and *C. albicans*, with inhibition zones measuring 22 and 21 mm, respectively. This suggests that the nanoparticles exhibited strong inhibitory effects on these particular pathogens. *S. epidermidis* and *S. aureus* also displayed relatively high inhibition zones, measuring 18 mm and 16 mm, respectively (Fig. 5). On the other hand, the lowest inhibition zone of 12 mm was observed against *P. aeruginosa*, indicating a comparatively weaker antimicrobial activity of the nanoparticles against this particular pathogen.

In recent years, infections caused by pathogenic microbes like *Pseudomonas aeruginosa, Acinetobacter baumannii, Staphylococcus aureus, Staphylococcus epidermidis,* and *Candida albicans* have gained significant importance [39-41]. Over the past few years, there has been an observed increase in the resistance of microbial species to antimicrobial agents. The restricted selection of antibacterial and antifungal drugs has become a significant concern when it comes to treating microbial diseases. The commonly

prescribed antimicrobial drugs have varying side effects, including lack of specificity and diminished efficacy in cancer patients undergoing chemotherapy, probiotic therapy, or taking anti-diabetic medications. Different research groups have created and examined different kinds of NPs, including various metal and metal-oxide-based nanoparticles. Examples of these nanoparticles are silver AgNPs, gold-oxide, ZnO, TiO_2, CuO, magnesium oxide (MgO), silver oxide (Ag_2O), (CaO), (SiO_2), and iron oxide [42-44].

In this study, nanocomposites with a size range of approximately 32 to 40 nm were examined for their antimicrobial properties. The results demonstrated that the compound consisting of iron-silver and chitosan (Fe-Ag-CS NPs) exhibited the strongest synergistic effect as a potential anticaries agent against *P. aeruginosa, A. baumannii, S. aureus, S. epidermidis,* and *C. albicans*, primarily due to their low minimum inhibitory concentration (MIC) values.

These findings demonstrate the antimicrobial potential of Fe–Ag-CS NPs against the studied pathogenic microbes. The variation in MIC values suggests differences in the susceptibility of the microbes to the different nanoparticle formulations. Additionally, the higher MBC values suggest that the nanoparticles possess bactericidal properties at concentrations higher than the MIC, indicating their potential for effective bacterial eradication. Numerous studies have investigated the antimicrobial properties of iron nanoparticles (Fe-Ag-CS NPs) against various bacteria and fungi [19,45,46].

Recently, bacteria have developed drug resistance, making the treatment of infections unsuccessful with limited treatment options. Therefore, this study highlights the potential of nanocomposites, specifically the Iron-silver-chitosan nanocomposite, as an emerging drug for combating drug-resistant pathogens. With the rise of bacterial drug resistance and limited treatment options, the antimicrobial activity of nanocomposites provides a promising alternative. The study's results indicate that the iron-silver-chitosan nanocomposite exhibited superior antimicrobial effects against pathogenic microbes, demonstrating a synergistic effect that resulted in significant antibacterial and antifungal properties. These findings emphasize the potential of nanocomposites as a valuable tool in the fight against drug-resistant infections.

Author Contributions

All authors took part in conceptualization, methodology execution, resources, original draft preparation and editing.

Conflict of Interest

The authors declare that there is no conflict of interest regarding the publication of this paper.

References

1. Dadgostar P. Antimicrobial resistance: implications and costs. Infection and drug resistance, (2019); 3903-3910.
2. European Center for Disease Prevention and Control. Surveillance of antimicrobial resistance in Europe 2018. Stockholm: ECDC, (2019).
3. Prestinaci F, Pezzotti P, Pantosti A. Antimicrobial resistance: a global multifaceted phenomenon. Pathogens and global health, (2015); 109(7): 309-318.
4. Control CfD, Prevention. Antibiotic Resistance Threats in the United States, 2013 (http://www. cdc. gov/drugresistance/thr eat-report-2013/); and Vital Signs: Improving Antibiotic Use Among Hospitalized Patients. MMWR March, (2014); 763.
5. Chokshi A, Sifri Z, Cennimo D, Horng H. Global contributors to antibiotic resistance. Journal of global infectious diseases, (2019); 11(1): 36.
6. Ahmad A, Viljoen A, Chenia H. The impact of plant volatiles on bacterial quorum sensing. Letters in applied microbiology, (2015); 60(1): 8-19.
7. Al-Masaudi SB, Al-Maaqar SMS. Susceptibility of multidrug-resistant enteric pathogenic diarrheal Bacteria to Saudi Honey. Journal of King Abdulaziz University: Science, (2020); 32(1): 47-64.
8. Al-Maaqar SM, Al-Johny BO, Al-Sharif FD, Al-Shaeri M, AL-Kenani N, et al. Sensitivity of multidrug-resistant pathogenic bacteria to ethanolic extract of Ziziphus spina-christi L. (Sidr) leaves. Bioscience Research (2022); 19(3): 1467-1475.
9. Kirui DK, Weber G, Talackine J, Millenbaugh NJ. Targeted laser therapy synergistically enhances efficacy of antibiotics against multi-drug resistant Staphylococcus aureus and Pseudomonas aeruginosa biofilms. Nanomedicine: Nanotechnology, Biology and Medicine, (2019); 20102018.
10. Yousefi B, Eslami M, Ghasemian A, Kokhaei P, Sadeghnejhad A. Probiotics can really cure an autoimmune disease? Gene Reports, (2019); 15100364.
11. Khan S, Alam F, Azam A, Khan AU. Gold nanoparticles enhance methylene blue–induced photodynamic therapy: a novel therapeutic approach to inhibit Candida albicans biofilm. International journal of nanomedicine, (2012); 3245-3257.
12. Ashrafi M, Bayat M, Mortazavi SP, Hashemi SJ, Meimandipour A. Antimicrobial effect of chitosan silver copper nanocomposite on Candida albicans in immunosuppressive rats. Veterinary Clinical Pathology The Quarterly Scientific Journal, (2022); 16(61): 15-27.
13. Ashrafi M, Bayat M, Mortazavi P, Hashemi SJ, Meimandipour A. Antimicrobial effect of chitosan–silver–copper nanocomposite on Candida albicans. Journal of Nanostructure in Chemistry, (2020); 1087-95.
14. Mohammed MA, Syeda JT, Wasan KM, Wasan EK. An overview of chitosan nanoparticles and its application in non-parenteral drug delivery. Pharmaceutics, (2017); 9(4): 53.
15. Eslami M, Vahabi V, Peyghan AA. Sensing properties of BN nanotube toward carcinogenic 4-chloroaniline: a computational study. Physica E: Low-dimensional Systems and Nanostructures, (2016); 766-11.
16. Eslami M, Peyghan AA. DNA nucleobase interaction with graphene like BC3 nano-sheet based on density functional theory calculations. Thin Solid Films, (2015); 58952-56.
17. Palza H. Antimicrobial polymers with metal nanoparticles. International journal of molecular sciences, (2015); 16(1): 2099-2116.

18. Ismail RA, Sulaiman GM, Abdulrahman SA, Marzoog TR. Antibacterial activity of magnetic iron oxide nanoparticles synthesized by laser ablation in liquid. Materials Science and Engineering: C, (2015); 53286-297.
19. Pal S (2014) Antimicrobial activity of iron oxide nanoparticles.
20. Mohan P, Mala R. Comparative antibacterial activity of magnetic iron oxide nanoparticles synthesized by biological and chemical methods against poultry feed pathogens. Materials Research Express, (2019); 6(11): 115077.
21. Burduşel A-C, Gherasim O, Grumezescu AM, Mogoantă L, Ficai A, et al. Biomedical applications of silver nanoparticles: an up-to-date overview. Nanomaterials, (2018); 8(9): 681.
22. Youssef A, Mohamed S, Abdel-Aziz M, Abdel-Aziz M, Turky G, et al. Biological studies and electrical conductivity of paper sheet based on PANI/PS/Ag-NPs nanocomposite. Carbohydrate polymers, (2016); 147333-343.
23. Kulatunga D, Dananjaya S, Godahewa G, Lee J, De Zoysa M. Chitosan silver nanocomposite (CAgNC) as an antifungal agent against Candida albicans. Medical Mycology, (2017); 55(2): 213-222.
24. Rhim J-W, Hong S-I, Park H-M, Ng PK. Preparation and characterization of chitosan-based nanocomposite films with antimicrobial activity. Journal of agricultural and food chemistry, (2006); 54(16): 5814-5822.
25. Shahbazi Y, Shavisi N. Current advancements in applications of chitosan based nano-metal oxides as food preservative materials. Nanomedicine Research Journal, (2019); 4(3): 122-129.
26. Mirhashemi AH, Bahador A, Kassaee MZ, Daryakenari G, Ahmad-Akhoundi MS, et al. Antimicrobial effect of nano-zinc oxide and nano-chitosan particles in dental composite used in orthodontics. Journal of Medical Bacteriology, (2013); 2(3-4): 1-10.
27. Vasylkiv O, Bezdorozhev O, Sakka Y. Synthesis of iron oxide nanoparticles with different morphologies by precipitation method with and without chitosan addition. Journal of the Ceramic Society of Japan, (2016); 124(4): 489-494.
28. Freire PL, Albuquerque AJ, Farias IA, da Silva TG, Aguiar JS, et al. Antimicrobial and cytotoxicity evaluation of colloidal chitosan–silver nanoparticles–fluoride nanocomposites. International journal of biological macromolecules, (2016); 93896-903.
29. Soares PI, Machado D, Laia C, Pereira LC, Coutinho JT, et al. Thermal and magnetic properties of chitosan-iron oxide nanoparticles. Carbohydrate polymers, (2016); 149382-390.
30. Elshikh M, Ahmed S, Funston S, Dunlop P, McGaw M, et al. Resazurin-based 96-well plate microdilution method for the determination of minimum inhibitory concentration of biosurfactants. Biotechnology letters, (2016); 38(6): 1015-1019.
31. Elshikh M, Ahmed S, Funston S, Dunlop P, McGaw M, et al. Resazurin-based 96-well plate microdilution method for the determination of minimum inhibitory concentration of biosurfactants. Biotechnology letters, (2016); 381015-1019.
32. Mustapha S, Ndamitso M, Abdulkareem A, Tijani J, Shuaib D, et al. Comparative study of crystallite size using Williamson-Hall and Debye-Scherrer plots for ZnO nanoparticles. Advances in Natural Sciences: Nanoscience and Nanotechnology, (2019); 10(4): 045013.
33. Gomathi M, Rajkumar P, Prakasam A. Study of dislocation density (defects such as Ag vacancies and interstitials) of silver nanoparticles, green-synthesized using Barleria cristata leaf extract and the impact of defects on the antibacterial activity. Results in Physics, (2018); 10858-864.
34. Unsoy G, Yalcin S, Khodadust R, Gunduz G, Gunduz U. Synthesis optimization and characterization of chitosan-coated iron oxide nanoparticles produced for biomedical applications. Journal of Nanoparticle Research, (2012); 141-13.
35. Kalarical Janardhanan S, Ramasamy I, Nair BU. Synthesis of iron oxide nanoparticles using chitosan and starch templates. Transition Metal Chemistry, (2008); 33127-131.
36. Sarkar S, Das R. Synthesis of silver nano-cubes and study of their elastic properties using X-ray diffraction line broadening. Journal of Nondestructive Evaluation, (2019); 381-8.
37. Nikpour M, Rabiee S, Jahanshahi M. Synthesis and characterization of hydroxyapatite/chitosan nanocomposite materials for medical engineering applications. Composites Part B: Engineering, (2012); 43(4): 1881-1886.
38. Jayalekshmi A, Victor SP, Sharma CP. Magnetic and degradable polymer/bioactive glass composite nanoparticles for biomedical applications. Colloids and Surfaces B: Biointerfaces, (2013); 101196-204.
39. Rui D, Rui R, Liu YL, Ying Z, Guo LN, et al. Causative Microorganisms Isolated from Patients with Intra-Abdominal Infections and Their Drug Resistance Profiles: An 11-Year (2011–2021) Single-Center Retrospective Study. Biomedical and Environmental Sciences, (2023); 36(8): 732-742.
40. Mariani F, Galvan EM. Staphylococcus aureus in Polymicrobial Skinand Soft Tissue Infections: Impact of Inter-Species Interactionsin Disease Outcome. Antibiotics, (2023); 12(7): 1164.
41. Talapko J, Juzbašić M, Matijević T, Pustijanac E, Bekić S, et al. Candida albicans—the virulence factors and clinical manifestations of infection. Journal of Fungi, (2021); 7(2): 79.
42. Seddighi NS, Salari S, Izadi AR. Evaluation of antifungal effect of iron-oxide nanoparticles against different Candida species. Iet Nanobiotechnology, (2017); 11(7): 883-888.
43. Rudramurthy GR, Swamy MK, Sinniah UR, Ghasemzadeh A. Nanoparticles: alternatives against drug-resistant pathogenic microbes. Molecules, (2016); 21(7): 836.
44. Ahmad A, Wei Y, Syed F, Tahir K, Rehman AU, et al. The effects of bacteria-nanoparticles interface on the antibacterial activity of green synthesized silver nanoparticles. Microbial pathogenesis, (2017); 102133-142.
45. Arias LS, Pessan JP, Vieira APM, Lima TMTd, Delbem ACB, et al. Iron oxide nanoparticles for biomedical applications: A perspective on synthesis, drugs, antimicrobial activity, and toxicity. Antibiotics, (2018); 7(2): 46.
46. Lavaee F, Faez K, Faez K, Hadi N, Modaresi F. Antimicrobial and antibiofilm activity of silver, titanium dioxide and iron nano particles. Am J Dent, (2016); 29(6): 315-320.